Article

Cell Reports

Compartment-Specific Biosensors Reveal a Complementary Subcellular Distribution of Bioactive Furin and PC7

Graphical Abstract

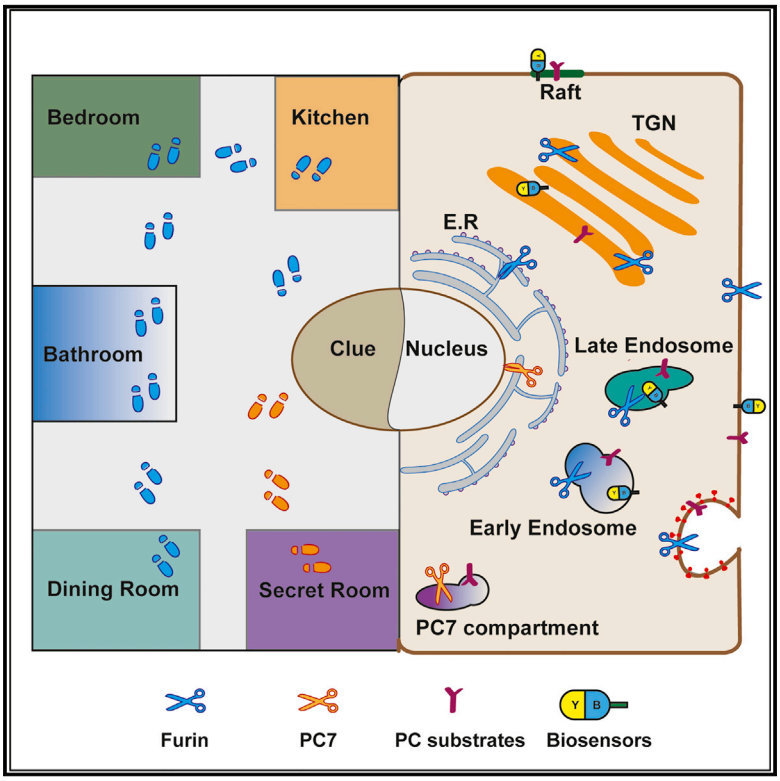

Authors

Pierpaolo Ginefra, Bruno G.H. Filippi, Prudence Donovan, Sylvain Bessonnard, Daniel B. Constam

Correspondence

daniel.constam@epfl.ch

In Brief

Using CRISPR editing of the proprotein convertases Furin and PC7 in B16F1 melanoma cells, combined with CLIP imaging of their activities at endogenous levels and after overexpression, Ginefra et al. reveal that differential subcellular distribution in the TGN/endosomal system regulates PC substrate specificities.

Highlights

- Variants of the biosensor CLIP can image PC activity at subcellular resolution
- Localization is rate limiting for how efficiently a given PC substrate is hydrolyzed
- Furin is less active in the TGN and more sensitive to inhibitor than in endosomes
- Overexpression enables PC7 recycling from early/late endosomes to the TGN

Ginefra et al., 2018, Cell Reports *22*, 2176–2189
February 20, 2018
https://doi.org/10.1016/j.celrep.2018.02.005

CellPress

OPEN ACCESS
CellPress

Cell Reports
Article

Compartment-Specific Biosensors Reveal a Complementary Subcellular Distribution of Bioactive Furin and PC7

Pierpaolo Ginefra,[1] Bruno G.H. Filippi,[1] Prudence Donovan,[1] Sylvain Bessonnard,[1] and Daniel B. Constam[1,2,*]
[1]Ecole Polytechnique Fédérale de Lausanne (EPFL) SV ISREC, Station 19, 1015 Lausanne, Switzerland
[2]Lead Contact
*Correspondence: daniel.constam@epfl.ch
https://doi.org/10.1016/j.celrep.2018.02.005

SUMMARY

Furin trafficking, and that of related proprotein convertases (PCs), may regulate which substrates are accessible for endoproteolysis, but tools to directly test this hypothesis have been lacking. Here, we develop targeted biosensors that indicate Furin activity in endosomes is 10-fold less inhibited by decanoyl-RVKR-chloromethylketone and enriched >3-fold in endosomes compared to the *trans*-Golgi network (TGN). Endogenous PC7, which resists this inhibitor, was active in distinct vesicles. Only overexpressed PC7 activity reached the cell surface, endosomes, and the TGN. A PLC motif in the cytosolic tail of PC7 was dispensable for endosomal activity, but it was specifically required for TGN recycling and to rescue proActivin-A cleavage in Furin-depleted B16F1 melanoma cells. In sharp contrast, PC7 complemented Furin in cleaving Notch1 independently of PLC-mediated TGN access. Our study provides a proof in principle that compartment-specific biosensors can be used to gain insight into the regulation of PC trafficking and to map the tropism of PC-specific inhibitors.

INTRODUCTION

Endoproteolytic cleavage by one or several proprotein convertases (PCs) determines the bioavailability of many secreted proteins in normal and cancerous tissues (Artenstein and Opal, 2011; Seidah and Prat, 2012). In common human cancers, such as lung adenocarcinoma and melanoma, the upregulation of PC activities correlates with tumor invasiveness (Bassi et al., 2001b; Fu et al., 2013; Lalou et al., 2010). Furthermore, PC inhibition can reduce proliferation and metastasis formation in several types of cancer *in vitro* and *in vivo* (Bassi et al., 2001a, 2010; Scamuffa et al., 2008). In other tumors, such as intestinal adenoma and hepatocellular carcinoma, PCs may be protective (Huang et al., 2012; Sun et al., 2009), and their inhibition enhances metastasis formation in colon cancer (Nejjari et al., 2004). Therefore, monitoring PC activities and the regulation of their specific oncogenic or tumor-suppressive functions will be critical to estimate the potential of pharmacological inhibitors in animal models of future cancer therapies.

Defining specific functions of individual PCs is complicated due to overlapping substrate specificities and partial redundancy among multiple family members (Bessonnard et al., 2015; Mesnard and Constam, 2010; Roebroek et al., 2004). Four of nine conserved PCs, including Furin, Pace4, PC5A/B, and PC7, cleave substrates after the minimal dibasic recognition motif (K/R)-(X)n-(K/R)↓, where n is 0, 2, 4, or 6 and X can be any amino acid (Seidah et al., 2008). In 152 PC sequences examined across species, the catalytic sites are 95% identical (Turpeinen et al., 2011), raising the question of why not all PCs always cleave the same substrates. PCs differ from each other mainly in their C-terminal cytosolic tails, which regulate trafficking in exocytic and endocytic vesicles by specific adaptor proteins (Seidah et al., 2008). After autocleavage, PCs exit the endoplasmatic reticulum (ER). However, they remain bound to their inhibitory cleaved prosegments in latent form until arrival at the cell surface or, in the case of Furin, in acidic endosomes (Anderson et al., 1997, 2002; Creemers et al., 1995; Mayer et al., 2003; Seidah et al., 2008), probably to avoid precocious activation or degradation of their substrates. Activated Furin and PC7 can then recycle from endosomes to the *trans*-Golgi network (TGN) by binding to specific adaptors in the cytosol (Chia et al., 2011; Declercq et al., 2012, 2017; Wan et al., 1998). Therefore, the substrate specificity of PCs likely depends on the relative enrichment of their bioactive forms in distinct subcellular compartments. However, tools to quantify total and individual PC activities in specific exocytic or endocytic vesicles are lacking.

To monitor the distribution of PC activities at the tissue level, we previously introduced the biosensor CLIP (cell-linked indicator of proteolysis). The initial version (v.)1 of CLIP consisted of secreted ECFP fused to membrane-bound Citrine via the sequence Arg-Gln-Arg-Arg (RQRR). Cleavage of this motif by Furin, PC7, Pace4, or Pcsk5 during and after exocytosis can be estimated by measuring ECFP/Citrine fluorescence ratios of CLIP v.1 at the cell surface (Bessonnard et al., 2015; Mesnard and Constam, 2010; Mesnard et al., 2011). However, ratiometric imaging underestimates the levels of uncleaved CLIP up to 2-fold because fluorescence resonance energy transfer (FRET) between the uncleaved fluorophores quenches ECFP and excites Citrine fluorescence (Clegg, 1992; VanEngelenburg and Palmer, 2008; Mesnard and Constam, 2010). Furthermore, the sensitivity of CLIP v.1 analysis is limited by the relatively weak fluorescence of ECFP, especially in tissues with high

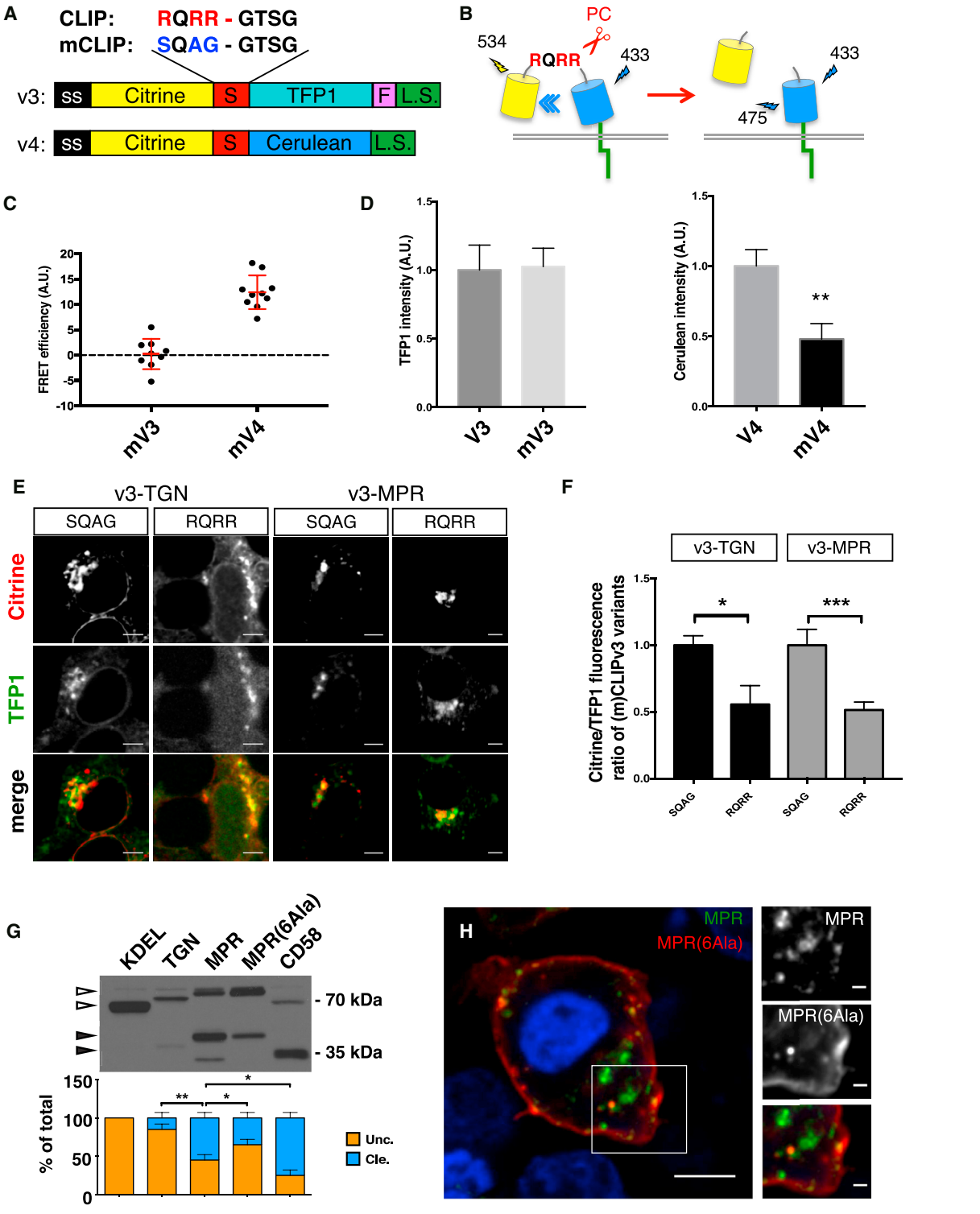

Figure 1. New Versions 3 and 4 of the Biosensor CLIP and Compartment-Specific Variants to Quantify Intracellular PC Activities by Ratiometric or FRET Imaging

(A) Schematic representation of the PC biosensors CLIP v.3 and v.4 and corresponding mCLIP control constructs where the PC recognition motif RQRR is mutated to SQAG to block cleavage (Mesnard and Constam, 2010). Compartment-specific variants were derived by adding specific localization signals (LSs). ss, secretory signal sequence; S, flexible linker comprising the PC cleavage site; F, FLAG epitope.

(legend continued on next page)

autofluorescence, and with ECFP and Citrine as a FRET pair, the acceptor donor/ratio in cells varies depending on pH and ion concentrations (Salonikidis et al., 2011).

To address these limitations, we here introduce CLIP v.3 and v.4. We show that CLIP v.3 is suitable for ratiometric imaging without interference by FRET, whereas CLIP v.4 can be used as a FRET-based biosensor to quantify PC activities in specific intracellular vesicles. By imaging compartment-specific variants of CLIP v.4 in PC-deficient melanoma cell lines engineered by CRISPR editing, we map the spatial distribution and relative contributions of endogenous Furin and PC7 activity. Besides establishing CLIP v.3 and CLIP v.4 as versatile PC biosensors, our results reveal a non-overlapping complementary distribution of endogenous bioactive Furin and PC7.

RESULTS

CLIP v.3 and v.4 and Their Variants Containing Distinct Localization Signals for Enrichment in Alternative Subcellular Compartments

The initial version (v.1) of CLIP and a mutant control (mCLIP) without a PC cleavage motif are enriched at the cell surface by the glycosylphosphatidyl-inositol (GPI) anchor of CD58 (Bessonnard et al., 2015; Mesnard and Constam, 2010). To improve the signal-to-noise ratio of CLIP v.1 fluorescence, we replaced the FRET donor (ECFP) by monomeric TFP1-FLAG or by monomeric Cerulean (Rizzo et al., 2006; Salonikidis et al., 2011), and we exchanged its position relative to monomeric Citrine (Figures 1A and 1B). Of the resulting CLIP v.3 and v.4, we derived several variants by replacing the GPI anchor with the transmembrane domains (TMDs) and cytosolic tails of membrane proteins containing well-defined trafficking signals (Table S1). To generate PC-resistant mCLIP controls that are needed for signal normalization of RQRR-specific cleavage, we mutated the RQRR linker sequences in all CLIP v.3 and CLIP v.4 variants to SQAG.

To verify that alternative trafficking signals are functional, we monitored Citrine epifluorescence of mCLIP v.3 variants in transfected HEK293T cells that were co-labeled for specific markers by immunofluorescent staining. As described for CLIP v.1 (Mesnard and Constam, 2010), targeting by the GPI signal enriched mCLIP v.3 at the plasma membrane (Figure S1A). By contrast, fusion to a C-terminal KDEL sequence retained mCLIP v.3 in the ER (Lewis and Pelham, 1990) (Figure S1B). Alternatively, fusion to the TMD and cytosolic tail of the TGN protein TGN38 (Bos et al., 1993) enriched mCLIP v.3 in vesicles stained for TGN46 (Figure S1C), whereas fusion of mCLIP v.3 to the TMD and cytosolic tail of CD-MPR led to its co-localization with the endogenous late endosomal protein CI-MPR (Ghosh et al., 2003) (Figure S1D). These results show that the localization signals examined are functional and enrich mCLIP v.3 in distinct specific subcellular compartments.

CLIP v.3 Cleavage and Ratiometric Imaging Can Estimate PC Activity in Exocytic Compartments

To estimate maximal FRET efficiencies of uncleaved CLIP v.3 and CLIP v.4, we compared PC-resistant mCLIP v.3 and mCLIP v.4 by sensitized emission analysis in transfected HEK293T cells, starting with CD-MPR-tagged variants (Figure S2). In mCLIP v.4, but not in the cleavable control CLIP v.4, excitation of Cerulean triggered strong Citrine emission while Cerulean emission was quenched by Citrine, indicating robust FRET specifically in the absence of cleavage (Figures 1C and 1D). By contrast, excitation of TFP1 as an energy donor for Citrine in mCLIP v.3 resulted in no FRET. Although unexpected, this confirms that the FRET signal of mCLIP v.4 was specific. Since mCLIP v.3 showed no FRET, we compared it to cleavable CLIP v.3 by ratiometric imaging. Irrespective of whether CLIP v.3 was targeted to the TGN or to late endosomes, its Citrine/TFP1 fluorescence ratio was 2-fold lower than in mCLIP v.3 controls, indicating cleavage (Figures 1E and 1F). However, ratiometry may underestimate PC activity in vesicles that do not release cleaved Citrine into the medium. To address this, we directly monitored CLIP v.3 cleavage by anti-FLAG western blot analysis of the membrane-anchored TFP1-FLAG moiety. Only 14% ± 5% of the total CLIP v.3-TGN in HEK293T cell lysates was actually cleaved, compared to 56% ± 5% of CLIP v.3-MPR and 73% ± 5% of GPI-anchored CLIP v.3-CD58 (Figure 1G). By contrast, CLIP v.3-KDEL containing the ER retention signal KDEL remained uncleaved. Besides confirming that endogenous PCs are activated in post-ER vesicles, these results show that the trafficking of a given substrate is rate limiting for its cleavage.

Since TGN38 and CD-MPR cycle between endosomes and TGN (Chia et al., 2011; Stöckli and Rohrer, 2004), biosensors that mimic their trafficking will not be cleaved in only one compartment. However, the baseline of cleavage at the plasma membrane and in early endosomes during rapid transit may be

(B) Shedding of Citrine by PCs is predicted to inhibit fluorescence resonance energy transfer (FRET) between excited donor (blue) and acceptor (yellow). Numbers, wavelengths (nm) of excitation and emission.

(C) Maximal normalized FRET efficiencies (NFRET) of mCLIP v.3 and mCLIP v.4 quantified by sensitized emission analysis in endosomes targeted by the localization signal of CD-MPR in live HEK293T cells. Data represent mean ± SEM of 2 experiments.

(D) TFP1 fluorescence of mCLIP v.3-MPR relative to that of CLIP v.3-MPR control (left), and Cerulean fluorescence of mCLIP v.4-MPR relative to CLIP v.4-MPR (right). Data represent mean ± SEM of 2 experiments (**$p < 0.01$, t test).

(E) Fluorescent images of CLIP v.3-TGN and CLIP v.3-MPR (RQRR) and their corresponding PC-resistant mCLIP v.3 controls (SQAG). Scale bars, 5 μm.

(F) Average Citrine/TFP1 fluorescence ratios of CLIP v.3-TGN and CLIP v.3-MPR relative to those of their mCLIP v.3 controls. Data represent mean ± SEM of 3 experiments (*$p < 0.05$ and ***$p < 0.001$, t test).

(G) Anti-FLAG western blot (top) of compartment-specific CLIP v.3 variants in HEK293T cell extracts. Densitometric analysis is shown below. Uncleaved (Unc.) and cleaved forms (Cle.) of CLIP v.3 variants fused to the indicated localization signals are marked in the top panel by open and closed arrowheads, respectively. Data represent mean ± SD (*$p < 0.05$ and **$p < 0.01$, t test).

(H) Epifluorescence of Citrine-MPR(6Ala) (red), which is enriched at the plasma membrane due to the endocytosis-blocking 6xAla mutation in the localization signal FFWYLL, and of the late endosomal marker Cerulean-MPR (green). Scale bars, 5 and 1 μm (inset). See also Figures S1 and S2 and Table S1.

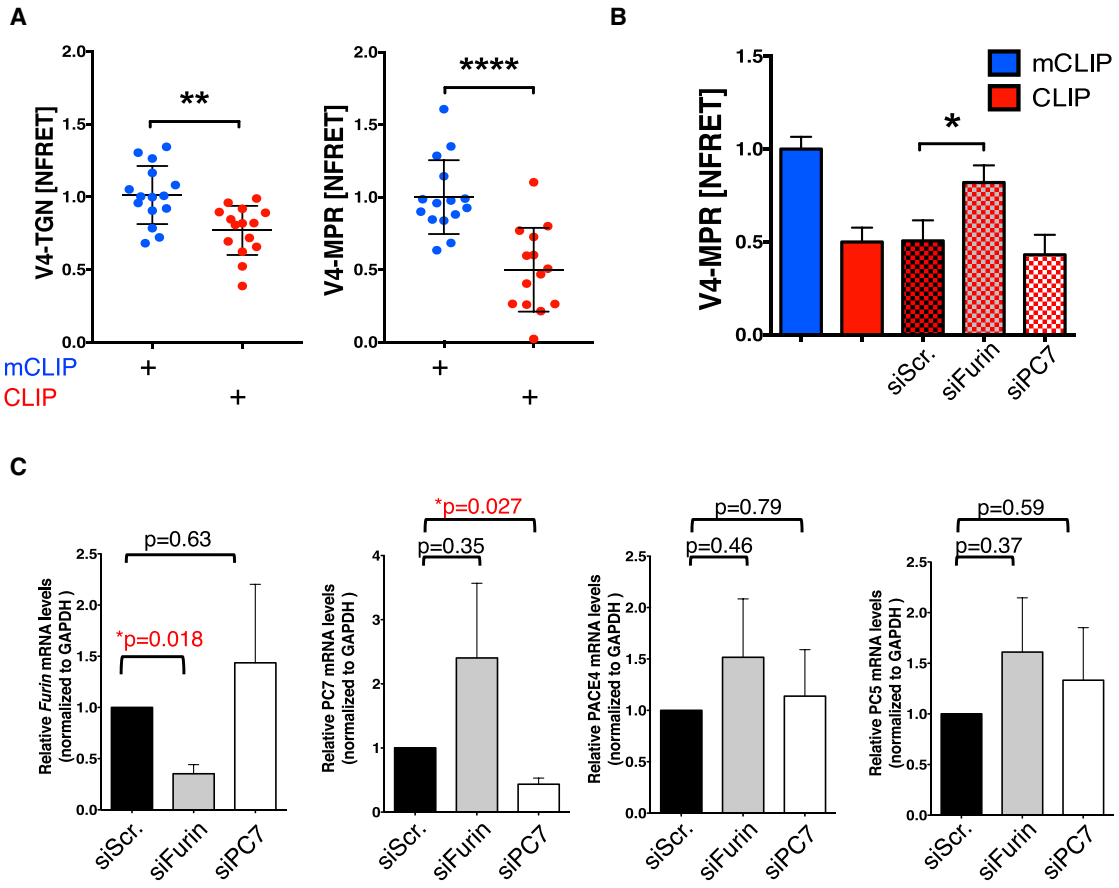

Figure 2. CLIP v.4 Cleavage Mediated by Endogenous Furin in HEK293T Cells Increases in Post-TGN Compared to TGN Vesicles

(A) Relative NFRET efficiencies of CLIP v.4-TGN and CLIP v.4-MPR. Each dot of the scatterplots represents the entire cytoplasmic region of one cell. Data represent mean ± SD (**p < 0.01 and ****p < 0.0001, t test).

(B) Relative NFRET efficiencies of CLIP v.4-MPR in HEK293T cells transfected with or without the indicated siRNAs. Data represent mean ± SD (*p < 0.05, t test).

(C) qRT-PCR analysis of endogenous PC mRNAs in wild-type HEK293T cells transfected with the indicated siRNAs. Asterisks mark significant differences relative to scrambled control (siScr) as determined by t test (p values are indicated). Data represent mean ± SEM. See also Figure S2.

similar for all CLIP variants and negligible compared to compartments where a sensor accumulates at steady state. To test this, we analyzed ^{35}S-labeled CLIP v.3 variants by pulse-chase analysis. If PC activity were uniformly distributed, CLIP v.3-TGN and CLIP v.3-MPR should be cleaved at comparable rates. Contrary to this prediction, analysis in stably transduced HeLa and HEK293T cells showed that, while it takes more than 4 hr to cleave half of CLIP v.3-TGN, half of CLIP v.3-MPR was processed within less than 1 hr (Figures S1E and S1F). These data suggest that PC activity is enriched in post-TGN compartments. To estimate cleavage of CLIP v.3-MPR before endocytosis, we analyzed the mutant derivative CLIP v.3-MPR(6Ala) that cannot interact with the clathrin machinery and, therefore, leaks to the cell surface (Ghosh et al., 2003; Stöckli and Rohrer, 2004) (Figure 1H). CLIP v.3-MPR(6Ala) was significantly less processed than its wild-type counterpart (Figure 1G; 36% ± 5% versus 56% ± 5%; $p < 0.05$) and at a slow rate similar to CLIP v.3-TGN (Figure S1F). These data show that CLIP v.3 cleavage correlates with its enrichment in different compartments, accelerating specifically in endosomes.

FRET Imaging of CLIP v.4 Confirms that Endogenous Furin Activity in HEK293T Cells Is Enriched in Endosomes Compared to the TGN

We were surprised that CLIP v.3 appeared up to 4-fold more cleaved in post-TGN compartments than in the TGN. To validate this conclusion and to rule out artifacts linked to protein turnover, we quantified total PC activity in these and other compartments by FRET imaging of CLIP v.4 variants. Their average FRET signals were normalized to the average maximal FRET of the corresponding non-cleavable mCLIP v.4 variants. By applying masks to measure entire cells (Figure S2), we found that the normalized FRET (NFRET) efficiency of CLIP v.4-TGN was only 25% ± 5% below that of PC-resistant mutant control mCLIP v.4-TGN (Figure 2A, left panel). By contrast, the average NFRET of CLIP v.4-MPR differed from that of mCLIP v.4-MPR by almost 50% ± 10% (right panel). These data corroborate our conclusion that total PC activity is significantly higher in late endosomes and/or other post-TGN compartments than in the TGN.

HEK293T cells transcribe five PC family members (Bessonnard et al., 2015). To obtain an initial estimate of their relative

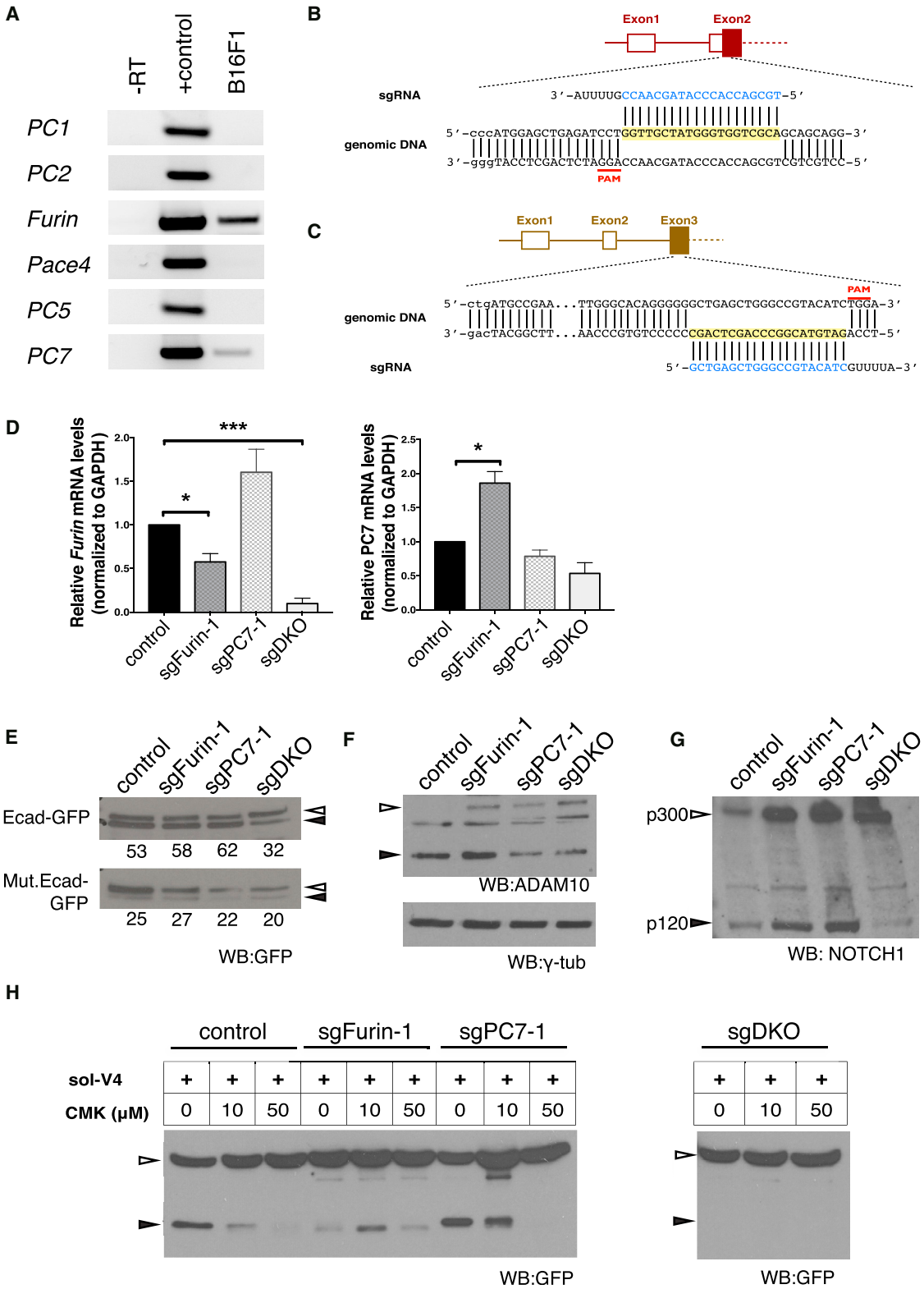

Figure 3. CRISPR/Cas9 Genome Editing of *Furin* and *PC7* in B16F1 Melanoma Cells

(A) RT-PCR analysis of PC mRNAs in B16F1 cells. Results are representative of 3 experiments.

(B) Targeted region of mouse *Furin* and sequences of two frameshift mutant alleles in the clone sgFurin-1. Yellow, targeted sequence; blue, complementary single guide RNA (sgRNA) sequence. Sequences of the resulting truncated protein products and anti-Furin western blot analysis are shown in Figure S3.

(legend continued on next page)

contributions to total PC activity during endocytosis, we depleted *Furin* or *PC7* mRNAs in HEK293T cells expressing CLIP v.4-MPR using previously validated small interfering RNAs (siRNAs) (Bessonnard et al., 2015; Scamuffa et al., 2008). Compared to cells transfected with scrambled control siRNA, cells depleted of 64% ± 10% of *Furin* mRNA significantly increased the average NFRET signal of CLIP v.4-MPR, whereas depletion of 56% ± 10% of *PC7* mRNA did not (Figure 2B). Depletion of Furin siRNA did not significantly increase PC7 mRNA levels (Figures 2B and 2C). Together, these results show that processing of the late endosomal PC biosensor CLIP v.4-MPR in HEK293T cells largely depends on Furin.

CRISPR/Cas9 Genome Editing of Endogenous PCs Expressed in B16F1 Melanoma Cells

Since multiple overlapping PC activities are coexpressed in most cells and tissues, their relative contributions to the cleavage of a given substrate are notoriously difficult to estimate. Tissue specificity and/or cross-regulation among PC family members may further complicate the interpretation of experimental manipulation (Bessonnard et al., 2015; Lapierre et al., 2007). To reduce this complexity, we decided to image compartment-specific CLIP v.4 variants in mouse B16F1 melanoma cells, which express endogenous *Furin* and *PC7* but no detectable *Pace4* or *PC5* mRNAs (Figure 3A). To inactivate endogenous Furin and PC7, we mutated their genes adjacent to the start codons in B16F1 cells using CRISPR/Cas9 genome editing (Figures 3B and 3C). Of 27 selected cell lines analyzed, 89% showed frameshift mutations in one or all alleles, resulting in premature stop codons and short inactive protein. We selected clones where no wild-type alleles were detected, including single-mutant sgPC7-1, sgFurin-1, and sgFurin-2 cells and double-knockout (sgDKO) cells (Figures S3A–S3C). Immunoblotting of cell extracts from wild-type and CRISPR-edited clones confirmed the loss of Furin protein expression specifically in sgFurin and sgDKO clones (Figure S3D). PC7 antibody is not commercially available. However, qRT-PCR analysis showed that sgFurin-1/2 and sgDKO clones continued to express PC7 mRNA or even significantly upregulated it compared to control cells (Figures 3D and S3E). Conversely, expression of *Furin* mRNA was reduced 2- or 10-fold in the sgFurin-1/2 and sgDKO clones, respectively, compared to control B16F1 cells, consistent with potential autoregulatory feedback (Blanchette et al., 2001; Qiu et al., 2015) (Figure 3D). Neither *Pace4* nor *PC5* was upregulated (data not shown). These data suggest that B16F1 melanoma cells are viable independently of Furin and PC7 but that loss of one of these PCs may influence the expression of the other.

To verify that endogenous Furin and PC7 in B16F1 cells were functional, we analyzed processing of known substrates. First, we transfected parental cells and CRISPR clones with E-cadherin, a validated *in vivo* substrate of overlapping Furin, PC7, and Pace4 activities (Bessonnard et al., 2015). A cleavage mutant E-cadherin where the PC recognition motif RQKR was mutated to SQAG served as a specificity control. Western blot analysis showed that 53%–62% of the stably accumulating total E-cadherin was cleaved in B16F1 sgFurin, sgPC7, and control cells, compared to only 32% in DKO. The residual cleaved fraction of 32% in DKO was close to the 20%–27% observed with SQAG mutant E-cadherin in B16F1 cells irrespective of their genotype (Figure 3E), indicating that it originated from PC-independent degradation. Thus, endogenous Furin and PC7 substitute for each other to cleave E-cadherin in B16F1 cells, similar to what we observed previously in mouse blastocysts (Bessonnard et al., 2015). Other substrates shared by Furin and PC7 may include the precursors of Notch1 and the disintegrin metalloproteinase proADAM10 (Anders et al., 2001; Logeat et al., 1998). Western blot analysis detected endogenous ADAM10 mainly in its mature form in control cells, whereas sgFurin-1, sgPC7-1, and sgDKO clones all enriched the uncleaved proform (Figure 3F). Analysis of endogenous Notch1 was hampered by a frequent loss of expression in CRISPR clones (data not shown). However, western blot analysis of transfected Notch1 revealed cleaved Notch1 p120 fragment specifically in control and in single-mutant clones, whereas it was absent in sgDKO cells (Figure 3G). These results indicate that both endogenous Furin and PC7 are functional in B16F1 cells and able to substitute for each other during Notch1 and ADAM10 precursor processing.

CRISPR Editing and PC Inhibitor Treatments Reveal that Both Endogenous Furin and PC7 Cleave CLIP v.4 in B16F1 Cells

The RQRR linker that is shared by CLIP v.1, CLIP v.3, and CLIP v.4 variants is efficiently cleaved by endogenous Furin and PC7 (Bessonnard et al., 2015; Mesnard and Constam, 2010). However, CLIP v.1 and other GPI-anchored fluorophores, such as Citrine-CD58 and Cerulean-CD58, did not accumulate at the plasma membrane or in conditioned media of B16F1

(C) Targeted region of the mouse *PC7* locus and frameshifted mutant alleles in clone sgPC7-1. Sequences of the resulting truncated protein products are shown in Figure S3.

(D) qRT-PCR analysis of *Furin* and *PC7* mRNAs in wild-type, sgFurin-1, sg-PC7-1, and sgDKO B16F1 cells. Data represent mean ± SEM (*$p < 0.05$ and ***$p < 0.001$, t test).

(E) Western blot analysis of GFP-tagged wild-type E-cadherin (top) or cleavage mutant RQKR > SQAG derivative (bottom) in whole-cell lysates of parental and sgFurin, sgPC7, and sgDKO B16F1 cell lines. Filled and open arrowheads here and elsewhere indicate cleaved and uncleaved forms, respectively.

(F) Western blot analysis of endogenous ADAM10 protein processing in B16F1 clones of the indicated genotypes. γ-tubulin served as a loading control.

(G) Western blot analysis of Notch1 in B16F1 clones. Notch1(p120) and Notch1(p300) correspond to cleaved and uncleaved forms, respectively.

(H) Anti-GFP western blots of conditioned media of the indicated B16F1 cell lines transfected with soluble CLIP v.4 and treated with the pan-PC inhibitor decanoyl-Arg-Val-Lys-Arg-chloromethylketone (CMK) or empty vehicle. In keeping with a role for PC7, residual CLIP v.4 cleavage in sgFurin cells was resistant to CMK treatment (Bessonnard et al., 2015) and blocked after CRISPR editing of PC7 in sgDKO cells. Filled and open arrowheads indicate cleaved Citrine and uncleaved CLIP v.4, respectively. Both blots in (F) were generated and processed in parallel but on two separate gels to accommodate all samples. See also Figure S3.

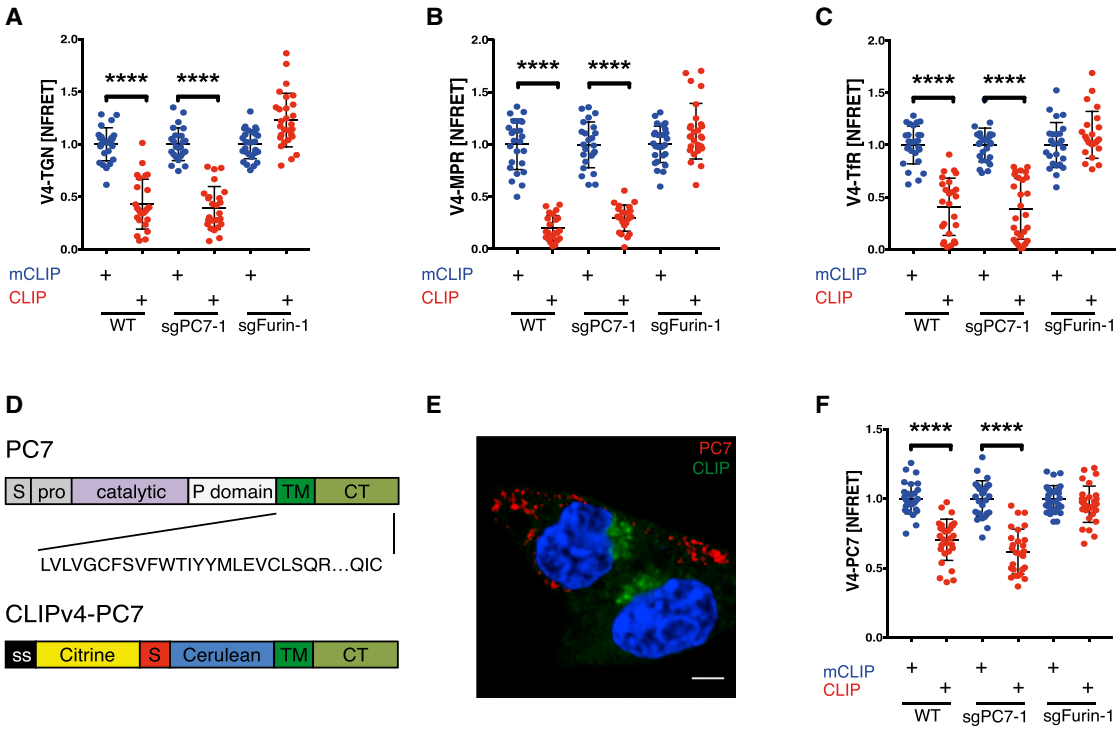

Figure 4. PC Activity in the TGN/Endosomal System Is Mediated by Furin, but Not by Endogenous PC7

(A–C) Average NFRET efficiencies of (A) CLIP v.4-TGN, (B) CLIP v.4-MPR, and (C) CLIP v.4-TfR in control, sgFurin-1, and sgPC7-1 B16F1 cells. Data represent mean ± SD (****$p < 0.0001$, t test).

(D) Schematic representation of the biosensor CLIP v.4-PC7 containing the TM domain and cytosolic tail of PC7 as a localization signal. Ss, secretory signal sequence; pro, propeptide; TM, transmembrane domain; CT, cytosolic tail.

(E) Immunofluorescent staining of FLAG-tagged mouse PC7 (red) in B16F1 cells shows no significant overlap with Citrine epifluorescence of mCLIP v.4-PC7 (green).

(F) Average NFRET efficiencies of CLIP v.4-PC7 in parental versus sgFurin-1 or sgPC7-1 B16F1 cells. Data represent mean ± SD (****$p < 0.0001$, t test). See also Figure S4.

cells (data not shown). Therefore, as an alternative control, we transfected B16F1 cells with a soluble secreted CLIP v.4 (CLIP v.4-sol) (Table S1). We found that sgFurin and sgPC7 single-mutant and control B16F1 cells all released uncleaved and cleaved CLIP v.4-sol into the medium, and mutation of *Furin* reduced or, when combined with the loss of *PC7*, abolished cleavage (Figure 3H). Mutation of *PC7* alone did not diminish cleaved CLIP v.4 in culture medium but rather increased it, correlating with significant upregulation of *Furin* mRNA (Figure 3D). These data show that both Furin and PC7 cleave CLIP v.4.

To validate the contribution of PC7 by an independent approach that does not rely on clonal DKO cell lines, we took advantage of the fact that the PC inhibitor decanoyl-Arg-Val-Lys-Arg-chloromethylketone (CMK) potently inhibits PC7 in cell-free assays, but not in cells and tissues even at high dosage (Bessonnard et al., 2015; Jean et al., 1998). Treatment with CMK for 12 hr dose-dependently inhibited CLIP v.4 cleavage in parental and in sgPC7-1 B16F1 cells. By contrast, cleavage of CLIP v.4 in sgFurin-1 cells was not inhibited even at the maximal tolerated CMK dosage of 50 μM (Figure 3H). These results agree with our data from DKO B16F1 cells that CLIP v.4 cleavage involves the PC7 compartment.

All PC Activity Detected in the TGN/Endosomal System of B16F1 Cells Is Mediated by Furin, but Not by Endogenous PC7

Since PC7 resisted CMK treatment *in vivo*, we previously speculated that it may function in intracellular compartments distinct from Furin (Bessonnard et al., 2015). To test this, we compared CLIP v.4 variants in control B16F1 cells and in CRISPR-edited clones. In parental B16F1 cells and in clones that were mutated by sgPC7 or transfected with Cas9 alone (B16-Cas9), average NFRET of CLIP v.4-TGN and CLIP v.4-MPR only reached approximately 40% and 20%, respectively (Figures 4A, 4B, S4A, and S4B). By contrast, in two independent sgFurin clones, NFRET of CLIP v.4-TGN and CLIP v.4-MPR soared to maximal levels (Figures 4A, 4B, S4C, and S4D). These results suggest that PC activity is enriched in endosomes compared to the TGN also in B16F1 cells and mediated in both compartments by Furin and not by PC7.

Since endogenous PC7 activity was not detected in the TGN or in late endosomes, we asked whether it may function in early endosomes. To target early endosomes, CLIP v.4 and its cleavage mutant control were fused to the type II TMD and cytosolic N terminus of transferrin receptor (TfR) (Schlierf et al., 2000; van Dam et al., 2002). In addition, we inverted the relative

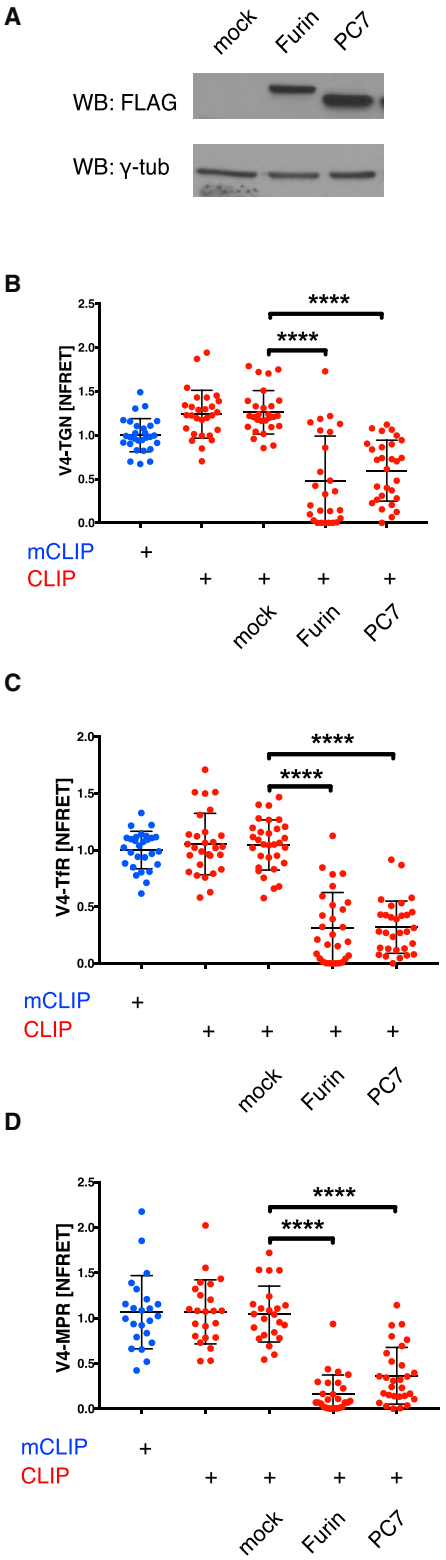

Figure 5. Overexpressed PC7 Activity in TGN/Endosomal Compartments

(A) Representative western blot of FLAG-tagged Furin or PC7 in extracts of sgDKO B16F1 cells. γ-tubulin served as a loading control.

(B–D) Live imaging of (B) CLIP v.4-TGN, (C) CLIP v.4-TfR, and (D) CLIP v.4-MPR in sgDKO B16F1 cells co-transfected with FLAG-tagged Furin or PC7. The asterisk indicates a significant difference with the mock control as determined by Mann-Whitney test. Data represent mean ± SD (****$p < 0.0001$). See also Figure S5.

positions of the fluorophores to retain the FRET donor at the membrane (Table S1; Figure S4E). Immunostaining confirmed that the resulting CLIP v.4-TfR co-localized with endogenous early endosome antigen-1 (EEA1) (Figure S4E). However, average NFRET of CLIP v.4-TfR only increased in sgFurin-1 and not in sgPC7-1 cells compared to B16F1 control (Figure 4C). These results suggest that endogenous PC activity in early endosomes of B16F1 cells is mediated by Furin and not by PC7.

Fusion to the Cytosolic Tail of PC7 Directs CLIP v.4 to Compartments that Harbor Furin Activity, but Not Full-Length PC7

To determine whether the PC7 compartment could be targeted by localization signals of PC7 itself, we fused CLIP v.4 to the cytosolic tail and TMD of PC7 (Figure 4D). Co-transfection of CLIP v.4-PC7 with FLAG-tagged PC7 resulted in no co-localization of the two proteins. Instead, anti-FLAG staining detected FLAG-PC7 in peripheral cytoplasmic vesicles, whereas CLIP v.4-PC7 showed a Golgi-like distribution near DAPI-stained nuclei (Figure 4E). Furthermore, sensitized emission analysis revealed that the average NFRET efficiencies of CLIP v.4-PC7 were 70% ± 3% and 60% ± 3% in B16F1 control and sgPC7-1 cells, respectively. By contrast, in sgFurin-1 cells, NFRET of CLIP v.4-PC7 increased to 95% ± 2% (Figure 4F). These results show that fusion to the TMD and cytosolic domains of PC7 does not route CLIP v.4 to endogenous PC7 but to alternative compartments that enable cleavage by Furin.

Overexpressed PC7 Cleaves TGN/Endosomal CLIP v.4 Variants

Previous work established that PC7 can be forced to travel to the cell surface by overexpression (Rousselet et al., 2011) and that overexpressed PC7 recycles to the TGN (Declercq et al., 2012, 2017; Rousselet et al., 2011; van de Loo et al., 1997), cleaving substrates during transit in endosomes (Guillemot et al., 2013). To monitor overexpressed PC7 activity in these compartments, we co-transfected sgDKO B16F1 cells with distinct CLIP v.4 variants and FLAG-PC7 or empty vector. FLAG-Furin was transfected as a control (Figure 5A). In all compartments analyzed that were devoid of detectable endogenous PC7 activity, overexpressed FLAG-PC7 reduced average NFRET of CLIP v.4 by >50%, similar to FLAG-Furin (Figures 5B–5D and S5A), suggesting overexpression can result in ectopic PC7 activity. To validate this conclusion, we analyzed tumor necrosis factor α-converting enzyme (TACE), also known as ADAM17, a known substrate of Furin and other PCs in the TGN (Endres et al., 2003; Srour et al., 2003). Western blot analysis detected uncleaved proADAM17 specifically in sgFurin-1 and in sgDKO, but not in sgPC7 or wild-type B16F1 cells (Figure S5B). Thus, endogenous PC7 failed to compensate for the loss of Furin during ADAM17 cleavage. Nevertheless, FLAG-PC7 overexpression readily restored

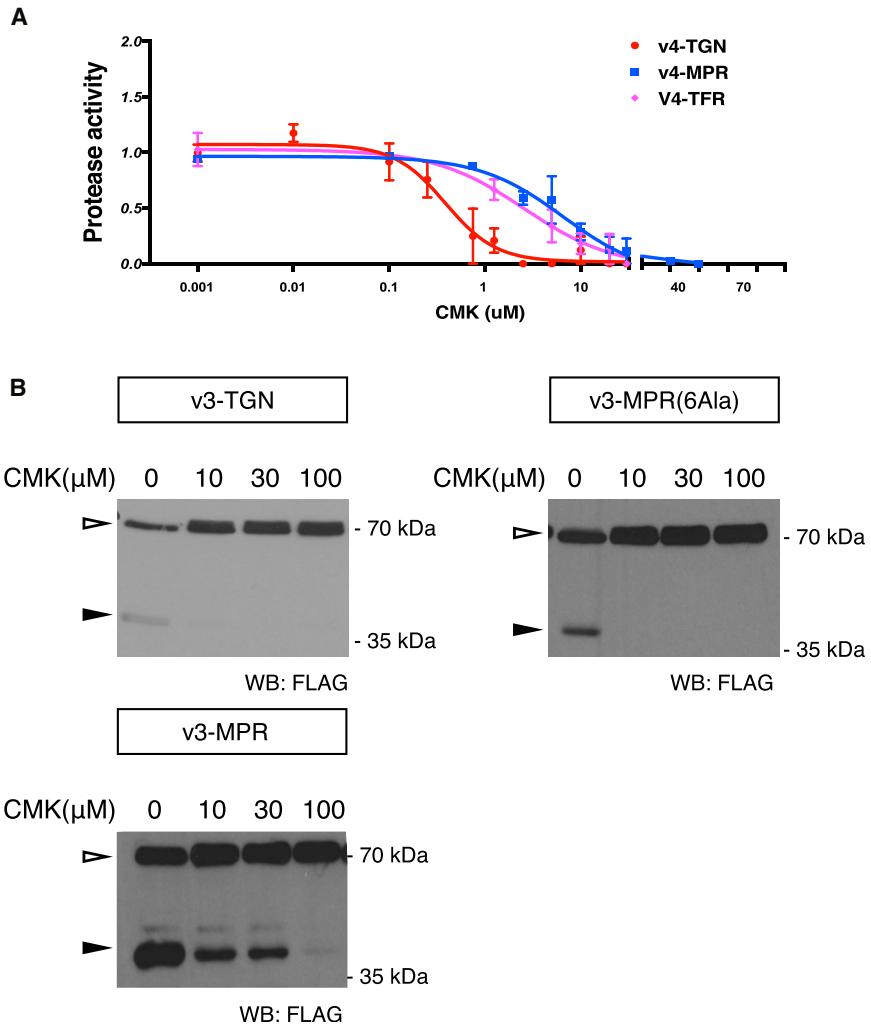

Figure 6. Tropism and Efficacy of the PC Inhibitor dec-RVKR-cmk in B16F1 Cells

(A) Inhibition of protease activity, plotted as the difference between mCLIP and CLIP NFRET efficiency, using increasing concentrations of the pan-PC inhibitor CMK in B16F1 cells. Data represent mean ± SD of 3 replicates, normalized to vehicle control and scaled to 1 of maximum activity.

(B) Anti-FLAG western blot analysis of CLIP v.3 in the TGN (v.3-TGN), at the plasma membrane (v.3-MPR[6Ala]), or in late endosomes (v.3-MPR) of HEK293T cells treated with the indicated dosage of CMK. Filled and open arrowheads indicate cleaved and uncleaved forms, respectively. See also Figure S6.

ADAM17 cleavage in sgDKO B16F1 cells similar to FLAG-Furin (Figure S5B). While endogenous PC7 is clearly active in B16F1 cells and functions redundantly with Furin, e.g., during Notch1 and ADAM10 cleavage (Figure 3), these results suggest that spatial compartmentalization is a likely determinant of substrate specificity.

Compartment-Specific Variants of the Biosensor CLIP v.4 Can Quantify the Efficacy of the PC Inhibitor CMK and Validate Its Access to Specific Intracellular Destinations

Besides elucidating the spatial distribution of PC activities, we reasoned that CLIP imaging might be useful to characterize the efficacy and tropism of PC inhibitors. As proof of principle, we compared CLIP v.4 variants in the TGN, early endosomes, and late endosomes of B16F1 cells treated with increasing concentrations of the inhibitor CMK. We found that CMK inhibited CLIP v.4 cleavage in the TGN with a half-maximum inhibitory concentration (IC_{50}) of 400 nM. By comparison, the IC_{50} concentrations of CMK required to inhibit CLIP v.4 in early or late endosomes were 3 and 7 μM, i.e., almost 10- or 20-fold higher dosages, respectively, than in the TGN (Figure 6A). To validate this difference across different cell types, we also titrated CMK on HEK293T cell lines stably expressing CLIP v.3-TGN, CLIP v.3-MPR, or the endocytosis-deficient mutant derivative CLIP v.3-MPR(6Ala). The results showed that, while a low concentration of 10 μM completely inhibited CLIP v.3 processing in the TGN and at the plasma membrane, a 10-fold higher dose (100 μM) was required to block cleavage in late endosomes (Figure 6B). The reduced sensitivity of CLIP v.4 to inhibition by CMK in endosomes compared to the TGN and plasma membrane corroborates our earlier conclusion that it is mainly cleaved locally within endosomes. Since Furin alone mediated cleavage of CLIP v.4 in all three compartments, CMK titration emerges as a convenient criterion to evaluate where a given Furin substrate is cleaved within the TGN/endosomal system.

To test this idea on a physiological Furin substrate, we focused on the pigment cell-specific-pre-melanosomal protein (PMEL, also known as PMEL17 or gp100), which is important for melanin synthesis and storage in melanocytes. Immature PMEL, called P1 form, is exported from the ER to the Golgi complex where its oligosaccharides are modified to derive the higher-molecular weight P2 form (Theos et al., 2005). The P2 form undergoes multiple proteolytic events, including PC-dependent cleavage, which is essential to generate functional melanosomes (Berson et al., 2003). Western blot analysis revealed that the P2 form was undetectable in parental cells but accumulated in sgFurin clones and in sgDKO (Figure S6A). This result indicates that Furin is the only PC able to process PMEL in B16F1 cells. Since PC cleavage of PMEL occurs during secretion independently of endocytic uptake (Leonhardt et al., 2011), we asked whether a low dose of CMK is sufficient to inhibit it. Confirming this prediction, the P2 form started to accumulate in cells treated with CMK concentration in the nanomolar range (Figure S6B),

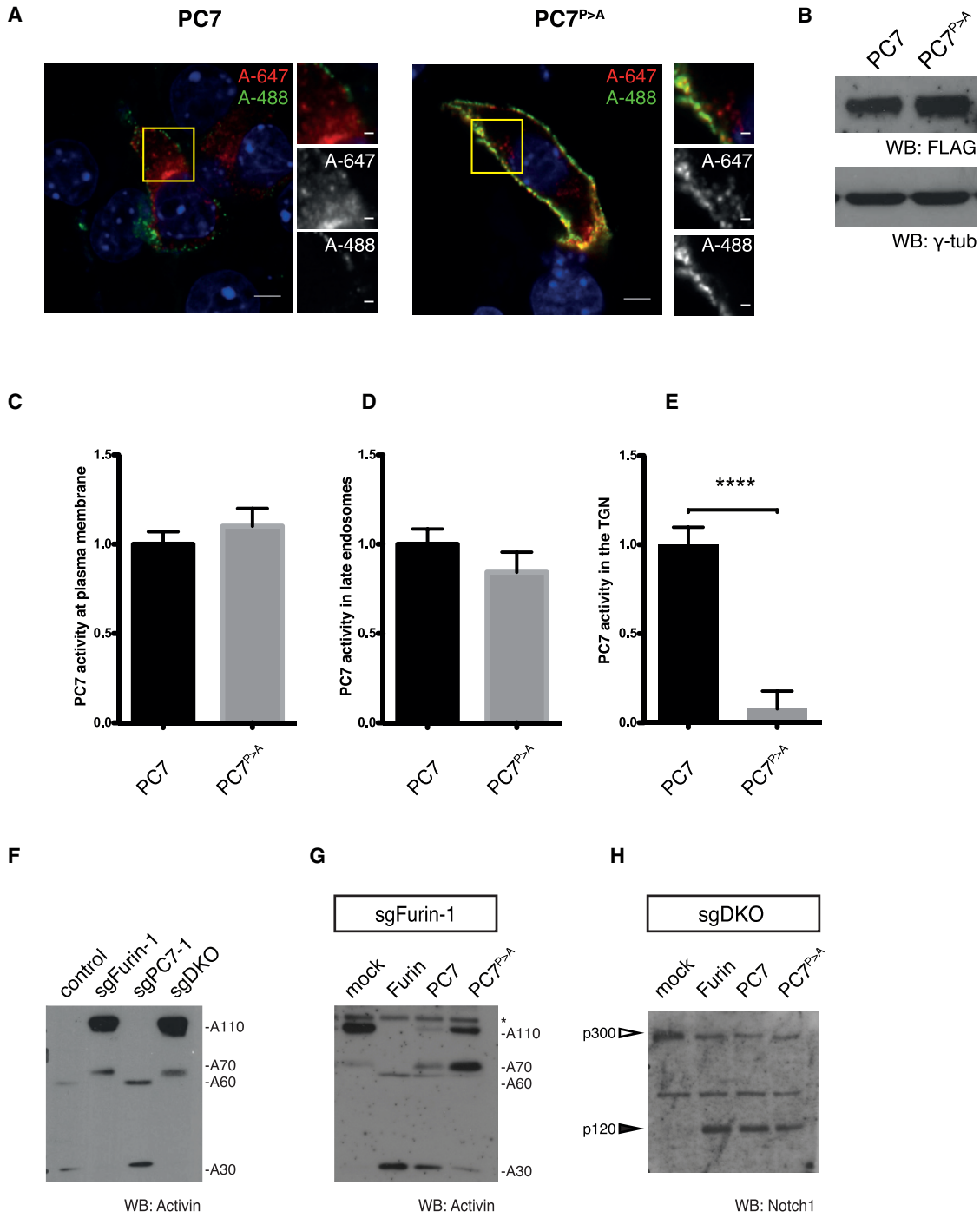

Figure 7. Internalization of Overexpressed PC7 Regulates Its Specificity

(A) Representative images of anti-FLAG M2 antibody internalized after 30 min at 4°C and 15 min at 37°C by sgDKO cells expressing wild-type PC7 (left) or mutant $PC7^{P>A}$ (right). Double immunofluorescent staining of FLAG-tagged PC7 before (green, A-488) and after cell permeabilization (red, A-647), respectively, distinguishes PC7 pools at the plasma membrane from those that were internalized. Scale bars, 5 and 1 μm (inset).

(B) Representative western blot of FLAG-tagged PC7 and $PC7^{P>A}$ in extracts of sgDKO B16F1 cells. γ-tubulin served as a loading control.

(C) Activity of $PC7^{P>A}$ relative to that of wild-type PC7 plotted as Citrine/TFP1 ratio difference in sgDKO cells co-expressing CLIP v.3 at the plasma membrane. The activity of wild-type PC7 was defined as 1.0 after normalization to empty vector control. Data represent mean ± SD.

(D and E) Activity of $PC7^{P>A}$ relative to that of wild-type PC7 plotted as NFRET difference in sgDKO cells co-expressing CLIP v.4 in (D) late endosomes or in (E) the TGN. The activity of wild-type PC7 was defined as 1.0 after normalization to empty vector control. The asterisk indicates a significant difference with the wild-type PC7 as determined by Mann-Whitney test. Data represent mean ± SD (****$p < 0.0001$).

(legend continued on next page)

i.e., at concentrations that are below those required to inhibit Furin activity in endosomes (Figure 6A). These data provide a proof of concept that pharmacological PC inhibitors can be used to differentially target a subset of diverse intracellular PC compartments.

Internalization of PC7 Is Required for Its Activity in Exocytic Compartments

Overexpressed PC7 uses both conventional and unconventional secretory pathways to reach the cell surface before internalization and recycling to the TGN (Declercq et al., 2012; Rousselet et al., 2011). A short sequence in the cytosolic tail composed of the residues Pro^{723}, Leu^{724}, and Cys^{725} is important to normally internalize PC7 from the plasma membrane. To test whether this internalization signal regulates PC7 function, we replaced Pro^{723}, Leu^{724}, and Cys^{725} in FLAG-tagged mouse PC7 by alanine residues. The resulting mutant $PC7^{P>A}$ or wild-type PC7 was expressed in B16F1, and defects in trafficking were evaluated by antibody uptake experiments using a double-labeling method as previously described (Declercq et al., 2012). Briefly, sgDKO cells expressing the FLAG-tagged wild-type or the FLAG-tagged mutant PC7 were incubated with anti-FLAG antibody for 30 min at 4°C and 15 min at 37°C, fixed, and stained with secondary antibodies. Plasma membrane-localized PC7 was stained green using a secondary Alexa488 antibody, while internalized PC7 was stained red using a secondary Alexa647 antibody. While the wild-type FLAG-tagged PC7 mediated efficient antibody uptake and enrichment in Golgi-like structures, the mutant $PC7^{P>A}$ accumulated at the cell surface, with few stained internalized vesicles (Figure 7A). Furthermore, anti-FLAG western blot analysis revealed no adverse effect of the PLC > AAA mutation on PC7 expression levels (Figure 7B). These results confirm that the PLC motif is important also in B16F1 cells to internalize overexpressed PC7 from the cell surface prior to its retrieval to the Golgi apparatus. To test potential effects on activity, we added back wild-type PC7 or $PC7^{P>A}$ mutant to sgDKO cells by co-transfection together with different CLIP v.4 variants or CLIP v.3-MPR(6Ala). While both wild-type PC7 and $PC7^{P>A}$ efficiently cleaved CLIP v.3 at the plasma membrane or CLIP v.4 in late endosomes, only wild-type PC7, but not $PC7^{P>A}$, rescued cleavage of CLIP v.4 in the TGN (Figures 7C–7E). These results suggest that PLC motif-mediated internalization is essential for overexpressed PC7 activity to reach exocytic vesicles of the TGN.

Spatial Mapping of Furin and PC7 Activities by Compartment-Specific CLIP v.4 Variants Can Explain Differential Substrate Specificities

Activin-A is a multifunctional endocrine factor related to transforming growth factor β (TGF-β). In syngeneic B16F1 melanoma grafts, autocrine growth-inhibitory Activin signaling is attenuated, while paracrine signaling promotes primary and metastatic growth by inhibiting tumor immunosurveillance (Donovan et al., 2017). However, how Activin-A precursor processing is regulated in this or other contexts is unknown (Antenos et al., 2008). To estimate the relative contributions of endogenous Furin and PC7 in Activin-A maturation, we transfected parental B16F1 cells and CRISPR clones with *INHβA* expression vector encoding Activin-A. Western blot analysis showed that conditioned media of control and sgPC7-1 single-mutant B16F1 cells accumulated mature Activin-A (A30) consisting of a homodimer of the C-terminal INHβA fragment (28–30 kDa), together with dimers of one cleaved and one uncleaved INHβA subunit (A60) (Huylebroeck et al., 1990; Mason et al., 1996), but no precursor dimers (A110). By contrast, in sgFurin-1 and sgDKO cells, A110 was stabilized, and the 60-kDa processing intermediate was shifted to 70 kDa (Figure 7G) or below detection (Figure 7G). To distinguish whether proActivin-A is intrinsically resistant to PC7 or whether it avoids endogenous PC7 compartments, we replenished sgFurin-1 cells with Furin (positive control) or with wild-type PC7 or its P > A mutant form that is active at the plasma membrane and in endosomes, but not in the TGN (Figures 7C–7E). Western blot analysis of conditioned media of cells co-transfected with *INHβA* confirmed that added-back Furin cleaved both the A110 and A70 forms of proActivin-A and rescued the release of A30 (Figure 7G). Cleavage of A110 and A70 was similarly rescued by overexpressed PC7, whereas the mutant $PC7^{P>A}$ cleaved both forms very inefficiently and barely rescued A30 secretion (Figure 7G). Thus, when forced to enter the TGN, PC7 clearly can convert A110 dimers to A30, whereas outside the TGN, PC7 only cleaves a single *INHβA* subunit to generate A70. In sharp contrast, PC7-mediated cleavage of proNotch1, a substrate shared by endogenous Furin and PC7 (Figure 3G), was unaffected by the P > A mutation (Figure 7H). The failure of $PC7^{P>A}$ to efficiently rescue A30 strongly suggests that conversion of A110 and A70 to A30 depends on sorting to the TGN.

DISCUSSION

PC trafficking likely regulates whether and where potential substrates are cleaved during or after exocytosis, but tools to directly test this hypothesis have been lacking. Here we investigated whether the biosensor CLIP that we invented to image endogenous PC activities in transgenic mice at the cell and tissue levels (Mesnard and Constam, 2010) can be modified to quantify PC activities and the tropism of specific inhibitors at subcellular resolution in intracellular vesicles. We found that the versions CLIP v.3 and CLIP v.4 and their variants carrying different localization signals can map PC activities in the TGN/endosomal system.

Besides validating CLIP v.3 and v.4 and their compartment-specific variants as ratiometric or FRET-based PC-specific biosensors, respectively, live imaging revealed increased PC activity in endosomes compared to exocytic vesicles in three

(F) Western blot analysis of conditioned media of the indicated B16F1 cells overexpressing Activin-A. Molecular weights of the cleaved products are indicated.
(G) Western blot analysis of conditioned media of sgFurin-1 cells overexpressing Activin-A and co-transfected with empty vector (mock) or the indicated PC. Molecular weights of the cleaved products are indicated (*non-specific band).
(H) Western blot analysis of sgDKO-1 cell lysates overexpressing Notch-1 and co-transfected with the indicated PC. Filled and open arrowheads indicate PC-cleaved Notch1(p120) and uncleaved Notch1(p300), respectively.

unrelated cell lines (HeLa, HEK293T, and B16F1 mouse melanoma). This was unexpected since immunolabelling previously associated Furin and PC7 with the TGN (Declercq et al., 2012, 2017; Rousselet et al., 2011; Schäfer et al., 1995; Teuchert et al., 1999). However, these studies focused on overexpressed proteins and did not distinguish latent from active PCs. Since Furin recycling to the TGN requires its cytosolic tail, which can be cleaved off by an unknown sheddase (Thomas, 2002), saturation of this sheddase by overexpressed Furin may increase recycling above physiological levels.

CRISPR editing revealed that both Furin and PC7 are functional in B16F1 cells and able to substitute for each other during Notch1 and ADAM10 precursor processing. Functional overlap with PC7 may explain why deletion of *Furin* alone is not sufficient to block Notch signaling in developing mouse embryos (Krebs et al., 2003; Raya et al., 2003; Roebroek et al., 1998). In B16F1 cells, manipulation of the localization of the shared reporter substrate CLIP v.4 revealed that endogenous Furin and PC7 are active in distinct vesicles. Differential sorting was predicted since PC7 and Furin partition to distinct density gradient fractions of ethanol-loaded rat livers (Wouters et al., 1998). In B16F1 cells, only overexpressed PC7 activity was detected in the TGN. Overexpressed PC7 recycles from the cell surface to the TGN also in other cell types (Declercq et al., 2012, 2017; Rousselet et al., 2011; van de Loo et al., 1997), cleaving substrates during transit in clathrin-coated endosomes (Guillemot et al., 2013). We found that mutation of a known recycling signal in the cytosolic tail of PC7 specifically blocked its activity in the TGN, but not at the cell surface or in endosomes. Thus, PC7 activity likely enters the TGN indirectly via the cell surface.

In HEK293 cells, overexpressed PC7 reaches the cell surface independently of coat protein II and the TGN and without inducing ER stress (Rousselet et al., 2011). If the TGN is forced to collapse with endosomes, overexpressed PC7 at the cell surface decreases by only 40%, and it still cleaves its inhibitory prosegment; however, the cleaved prosegment remains intracellular instead of being secreted (Rousselet et al., 2011). Possibly, PC7 cycles between the cell surface and endosomes to facilitate the release from cleaved prosegment before transport to the TGN. While not ruling out such retrograde transport in cells with elevated PC7 expression, our finding in B16F1 cells that endogenous bioactive PC7 failed to cleave TGN biosensors and to mimic Furin activity during ADAM17 cleavage (a known PC substrate in the TGN) suggests that TGN access was inefficient. Possibly, traffic via clathrin-coated endosomes to the TGN is limited by the sequestration of PC7 in uncoated Flotillin carriers (Rousselet et al., 2011).

A long-standing enigma is whether compartmentalization of PCs determines their substrate specificities. To address this question, we evaluated whether the spatial mapping of Furin and PC7 activities by CLIP v.4 imaging can explain which of these endogenous PCs, if any, mediates cleavage of the multifunctional Activin-A precursor. Activin-A regulates the menstrual cycle, bone and skeletal muscle formation (Chen et al., 2017), inflammatory processes (Hedger et al., 2011; Sanchez-Duffhues et al., 2015), and tumorigenesis (Loomans and Andl, 2014). Little is known about the processing of proActivin-A via partially cleaved intermediates and its regulation. Here we found that Furin, but not endogenous PC7, mediates the release of mature Activin-A by B16F1 cells. In cells lacking Furin, overexpressed wild-type PC7 efficiently rescued maturation. By contrast, mutant $PC7^{P>A}$ activity that is excluded from the TGN but remains functional at the plasma membrane and in endosomes only partially cleaved one subunit. These observations confirm the prediction of our biosensor data that PC localization is rate limiting for how efficiently a given substrate is hydrolyzed. These findings will be important to inform future strategies of how Furin and PC7 may be targeted pharmacologically to preferentially block the processing of unique or shared substrates, respectively.

EXPERIMENTAL PROCEDURES

Cell Lines

HEK293T, HeLa, and B16F1 melanoma cells (ATCC) were maintained in DMEM supplemented with 10% fetal bovine serum, 1% gentamicin, and 1% GlutaMAX (Gibco and Invitrogen). HEK293T and HeLa cells stably transduced with lentiviral CLIP v.3 reporter were maintained in the same medium supplemented with Puromycin (2 μg/mL) (Gibco and Invitrogen).

Ratiometric Imaging and FRET Analysis

For live-cell imaging, transfected cells on coverslips in 3.5-cm dishes were transferred in buffered OptiMEM while the temperature was maintained at 37°C throughout the imaging process. Single-cell images were acquired using a W N-Achromat 63×/0.9 objective on a confocal microscope (Zeiss LSM 710) at the following settings: Cerulean channel, 458-nm excitation and 460- to 510-nm emission; TFP1 channel, 458-nm excitation and 463- to 514-nm emission; FRET channel, 458-nm excitation and 530- to 600-nm emission; and Citrine channel, 514-nm excitation and 530- to 600-nm emission. NFRET efficiency was calculated as described (Xia and Liu, 2001) by normalizing the corrected FRET signal to the square root of the product between Cerulean and Citrine intensities. Owing to this normalization, NFRET is independent of local fluorophore concentration, and potential FRET between-cell-linked Cerulean and soluble Citrine trapped in vesicles was accounted for. Correction factors accounting for spectral bleed-through were determined independently on cells transfected with Cerulean or Citrine alone. Images of 5–15 reporter cells per condition were analyzed using ImageJ PixFRET plug-in to quantify NFRET in all regions defined by a mask of significant Cerulean signal above an arbitrary threshold (Feige et al., 2005) (Figure S2). Each dot of the scatterplot represents a single cell. For ratiometric analysis, the mean of TFP1 and Citrine background fluorescence was measured in untransfected cells. For each of the CLIP v.3-expressing cells, a mask was generated using the TFP1 channel and overlaid with the channels of interest (TFP1 and Citrine). Mean fluorescent intensities, after background subtraction, were measured, and Citrine values were divided with the corresponding TFP1 values to obtain individual Citrine/TFP1 ratios.

Statistical Analysis

Statistical tests were performed using Prism (GraphPad). Unless indicated otherwise, data represent mean ± SD of at least 3 independent experiments. The normal distributions of Citrine/TFP1 ratios and of normalized NFRET values were verified with the Shapiro-Wilk normality test, and the results were analyzed by Mann-Whitney or by Student's t test. IC_{50} values were calculated using Prism (GraphPad). A p value < 0.05 was considered significant.

SUPPLEMENTAL INFORMATION

Supplemental Information includes Supplemental Experimental Procedures, six figures, and one table and can be found with this article online at https://doi.org/10.1016/j.celrep.2018.02.005.

ACKNOWLEDGMENTS

We would like to thank Dr. Arne Seitz and his team at the EPFL bioimaging core facility for advice on image acquisition and analysis. This work was supported

by grants 3100A0-118080/1 and 31003A_156452 from the Swiss National Science Foundation to D.B.C. and by the ISREC Foundation grant 531846 to P.G.

AUTHOR CONTRIBUTIONS

B.G.H.F. and D.B.C. conceived the initial experiments. B.G.H.F. generated CLIP v.3 and CLIP v.4 variants and performed pulse-chase experiments. P.G. together with P.D. and B.G.H.F. characterized their distribution and cleavage in human cell lines. P.G. and S.B. generated CRISPR-edited *Furin*- and *PC7*-knockout alleles. P.G. cloned and imaged CLIP v.4 variants and, together with D.B.C., wrote the manuscript. P.G., B.G.H.F., and D.B.C. edited the manuscript.

DECLARATION OF INTERESTS

The authors declare no competing interests.

Received: July 21, 2017
Revised: December 13, 2017
Accepted: January 31, 2018
Published: February 20, 2018

REFERENCES

Anders, A., Gilbert, S., Garten, W., Postina, R., and Fahrenholz, F. (2001). Regulation of the alpha-secretase ADAM10 by its prodomain and proprotein convertases. FASEB J. *15*, 1837–1839.

Anderson, E.D., VanSlyke, J.K., Thulin, C.D., Jean, F., and Thomas, G. (1997). Activation of the furin endoprotease is a multiple-step process: requirements for acidification and internal propeptide cleavage. EMBO J. *16*, 1508–1518.

Anderson, E.D., Molloy, S.S., Jean, F., Fei, H., Shimamura, S., and Thomas, G. (2002). The ordered and compartment-specfific autoproteolytic removal of the furin intramolecular chaperone is required for enzyme activation. J. Biol. Chem. *277*, 12879–12890.

Antenos, M., Zhu, J., Jetly, N.M., and Woodruff, T.K. (2008). An activin/furin regulatory loop modulates the processing and secretion of inhibin α- and βB-subunit dimers in pituitary gonadotrope cells. J. Biol. Chem. *283*, 33059–33068.

Artenstein, A.W., and Opal, S.M. (2011). Proprotein convertases in health and disease. N. Engl. J. Med. *365*, 2507–2518.

Bassi, D.E., Lopez De Cicco, R., Mahloogi, H., Zucker, S., Thomas, G., and Klein-Szanto, A.J. (2001a). Furin inhibition results in absent or decreased invasiveness and tumorigenicity of human cancer cells. Proc. Natl. Acad. Sci. USA *98*, 10326–10331.

Bassi, D.E., Mahloogi, H., Al-Saleem, L., Lopez De Cicco, R., Ridge, J.A., and Klein-Szanto, A.J. (2001b). Elevated furin expression in aggressive human head and neck tumors and tumor cell lines. Mol. Carcinog. *31*, 224–232.

Bassi, D.E., Zhang, J., Cenna, J., Litwin, S., Cukierman, E., and Klein-Szanto, A.J. (2010). Proprotein convertase inhibition results in decreased skin cell proliferation, tumorigenesis, and metastasis. Neoplasia *12*, 516–526.

Berson, J.F., Theos, A.C., Harper, D.C., Tenza, D., Raposo, G., and Marks, M.S. (2003). Proprotein convertase cleavage liberates a fibrillogenic fragment of a resident glycoprotein to initiate melanosome biogenesis. J. Cell Biol. *161*, 521–533.

Bessonnard, S., Mesnard, D., and Constam, D.B. (2015). PC7 and the related proteases Furin and Pace4 regulate E-cadherin function during blastocyst formation. J. Cell Biol. *210*, 1185–1197.

Blanchette, F., Rudd, P., Grondin, F., Attisano, L., and Dubois, C.M. (2001). Involvement of Smads in TGFbeta1-induced furin (fur) transcription. J. Cell. Physiol. *188*, 264–273.

Bos, K., Wraight, C., and Stanley, K.K. (1993). TGN38 is maintained in the trans-Golgi network by a tyrosine-containing motif in the cytoplasmic domain. EMBO J. *12*, 2219–2228.

Chen, J.L., Walton, K.L., Hagg, A., Colgan, T.D., Johnson, K., Qian, H., Gregorevic, P., and Harrison, C.A. (2017). Specific targeting of TGF-β family ligands demonstrates distinct roles in the regulation of muscle mass in health and disease. Proc. Natl. Acad. Sci. *114*, E5266–E5275.

Chia, P.Z., Gasnereau, I., Lieu, Z.Z., and Gleeson, P.A. (2011). Rab9-dependent retrograde transport and endosomal sorting of the endopeptidase furin. J. Cell Sci. *124*, 2401–2413.

Clegg, R.M. (1992). Fluorescence resonance energy transfer and nucleic acids. Methods Enzymol. *211*, 353–388.

Creemers, J.W., Vey, M., Schäfer, W., Ayoubi, T.A., Roebroek, A.J., Klenk, H.D., Garten, W., and Van de Ven, W.J. (1995). Endoproteolytic cleavage of its propeptide is a prerequisite for efficient transport of furin out of the endoplasmic reticulum. J. Biol. Chem. *270*, 2695–2702.

Declercq, J., Meulemans, S., Plets, E., and Creemers, J.W. (2012). Internalization of proprotein convertase PC7 from plasma membrane is mediated by a novel motif. J. Biol. Chem. *287*, 9052–9060.

Declercq, J., Ramos-Molina, B., Sannerud, R., Brouwers, B., Pruniau, V.P.E.G., Meulemans, S., Plets, E., Annaert, W., and Creemers, J.W.M. (2017). Endosome to trans-Golgi network transport of Proprotein Convertase 7 is mediated by a cluster of basic amino acids and palmitoylated cysteines. Eur. J. Cell Biol. *96*, 432–439.

Donovan, P., Dubey, O.A., Kallioinen, S., Rogers, K.W., Muehlethaler, K., Müller, P., Rimoldi, D., and Constam, D.B. (2017). Paracrine Activin-A signaling promotes melanoma growth and metastasis through immune evasion. J. Invest. Dermatol. *137*, 2578–2587.

Endres, K., Anders, A., Kojro, E., Gilbert, S., Fahrenholz, F., and Postina, R. (2003). Tumor necrosis factor-alpha converting enzyme is processed by proprotein-convertases to its mature form which is degraded upon phorbol ester stimulation. Eur. J. Biochem. *270*, 2386–2393.

Feige, J.N., Sage, D., Wahli, W., Desvergne, B., and Gelman, L. (2005). PixFRET, an ImageJ plug-in for FRET calculation that can accommodate variations in spectral bleed-throughs. Microsc. Res. Tech. *68*, 51–58.

Fu, J., Bassi, D.E., Zhang, J., Li, T., Cai, K.Q., Testa, C.L., Nicolas, E., and Klein-Szanto, A.J. (2013). Enhanced UV-induced skin carcinogenesis in transgenic mice overexpressing proprotein convertases. Neoplasia *15*, 169–179.

Ghosh, P., Dahms, N.M., and Kornfeld, S. (2003). Mannose 6-phosphate receptors: new twists in the tale. Nat. Rev. Mol. Cell Biol. *4*, 202–212.

Guillemot, J., Canuel, M., Essalmani, R., Prat, A., and Seidah, N.G. (2013). Implication of the proprotein convertases in iron homeostasis: proprotein convertase 7 sheds human transferrin receptor 1 and furin activates hepcidin. Hepatology *57*, 2514–2524.

Hedger, M.P., Winnall, W.R., Phillips, D.J., and de Kretser, D.M. (2011). The Regulation and Functions of Activin and Follistatin in Inflammation and Immunity. In Vitamins and Hormones, L. Gerald, ed. (Academic Press), pp. 255–297.

Huang, Y.H., Lin, K.H., Liao, C.H., Lai, M.W., Tseng, Y.H., and Yeh, C.T. (2012). Furin overexpression suppresses tumor growth and predicts a better postoperative disease-free survival in hepatocellular carcinoma. PLoS ONE *7*, e40738.

Huylebroeck, D., Van Nimmen, K., Waheed, A., von Figura, K., Marmenout, A., Fransen, L., De Waele, P., Jaspar, J.M., Franchimont, P., Stunnenberg, H., et al. (1990). Expression and processing of the activin-A/erythroid differentiation factor precursor: a member of the transforming growth factor-beta superfamily. Mol. Endocrinol. *4*, 1153–1165.

Jean, F., Stella, K., Thomas, L., Liu, G., Xiang, Y., Reason, A.J., and Thomas, G. (1998). alpha1-Antitrypsin Portland, a bioengineered serpin highly selective for furin: application as an antipathogenic agent. Proc. Natl. Acad. Sci. USA *95*, 7293–7298.

Krebs, L.T., Iwai, N., Nonaka, S., Welsh, I.C., Lan, Y., Jiang, R., Saijoh, Y., O'Brien, T.P., Hamada, H., and Gridley, T. (2003). Notch signaling regulates left-right asymmetry determination by inducing Nodal expression. Genes Dev. *17*, 1207–1212.

Lalou, C., Scamuffa, N., Mourah, S., Plassa, F., Podgorniak, M.P., Soufir, N., Dumaz, N., Calvo, F., Basset-Seguin, N., and Khatib, A.M. (2010). Inhibition

of the proprotein convertases represses the invasiveness of human primary melanoma cells with altered p53, CDKN2A and N-Ras genes. PLoS ONE *5*, e9992.

Lapierre, M., Siegfried, G., Scamuffa, N., Bontemps, Y., Calvo, F., Seidah, N.G., and Khatib, A.M. (2007). Opposing function of the proprotein convertases furin and PACE4 on breast cancer cells' malignant phenotypes: role of tissue inhibitors of metalloproteinase-1. Cancer Res. *67*, 9030–9034.

Leonhardt, R.M., Vigneron, N., Rahner, C., and Cresswell, P. (2011). Proprotein convertases process Pmel17 during secretion. J. Biol. Chem. *286*, 9321–9337.

Lewis, M.J., and Pelham, H.R. (1990). A human homologue of the yeast HDEL receptor. Nature *348*, 162–163.

Logeat, F., Bessia, C., Brou, C., LeBail, O., Jarriault, S., Seidah, N.G., and Israël, A. (1998). The Notch1 receptor is cleaved constitutively by a furin-like convertase. Proc. Natl. Acad. Sci. USA *95*, 8108–8112.

Loomans, H.A., and Andl, C.D. (2014). Intertwining of Activin A and TGFβ Signaling: Dual Roles in Cancer Progression and Cancer Cell Invasion. Cancers (Basel) *7*, 70–91.

Mason, A.J., Farnworth, P.G., and Sullivan, J. (1996). Characterization and determination of the biological activities of noncleavable high molecular weight forms of inhibin A and activin A. Mol. Endocrinol. *10*, 1055–1065.

Mayer, G., Boileau, G., and Bendayan, M. (2003). Furin interacts with proMT1-MMP and integrin alphaV at specialized domains of renal cell plasma membrane. J. Cell Sci. *116*, 1763–1773.

Mesnard, D., and Constam, D.B. (2010). Imaging proprotein convertase activities and their regulation in the implanting mouse blastocyst. J. Cell Biol. *191*, 129–139.

Mesnard, D., Donnison, M., Fuerer, C., Pfeffer, P.L., and Constam, D.B. (2011). The microenvironment patterns the pluripotent mouse epiblast through paracrine Furin and Pace4 proteolytic activities. Genes Dev. *25*, 1871–1880.

Nejjari, M., Berthet, V., Rigot, V., Laforest, S., Jacquier, M.F., Seidah, N.G., Remy, L., Bruyneel, E., Scoazec, J.Y., Marvaldi, J., and Luis, J. (2004). Inhibition of proprotein convertases enhances cell migration and metastases development of human colon carcinoma cells in a rat model. Am. J. Pathol. *164*, 1925–1933.

Qiu, H., Tang, X., Ma, J., Shaverdashvili, K., Zhang, K., and Bedogni, B. (2015). Notch1 Autoactivation via Transcriptional Regulation of Furin, Which Sustains Notch1 Signaling by Processing Notch1-Activating Proteases ADAM10 and Membrane Type 1 Matrix Metalloproteinase. Mol. Cell. Biol. *35*, 3622–3632.

Raya, A., Kawakami, Y., Rodriguez-Esteban, C., Buscher, D., Koth, C.M., Itoh, T., Morita, M., Raya, R.M., Dubova, I., Bessa, J.G., et al. (2003). Notch activity induces Nodal expression and mediates the establishment of left-right asymmetry in vertebrate embryos. Genes Dev. *17*, 1213–1218.

Rizzo, M.A., Springer, G., Segawa, K., Zipfel, W.R., and Piston, D.W. (2006). Optimization of pairings and detection conditions for measurement of FRET between cyan and yellow fluorescent proteins. Microsc. Microanal. *12*, 238–254.

Roebroek, A.J., Umans, L., Pauli, I.G., Robertson, E.J., van Leuven, F., Van de Ven, W.J., and Constam, D.B. (1998). Failure of ventral closure and axial rotation in embryos lacking the proprotein convertase Furin. Development *125*, 4863–4876.

Roebroek, A.J., Taylor, N.A., Louagie, E., Pauli, I., Smeijers, L., Snellinx, A., Lauwers, A., Van de Ven, W.J., Hartmann, D., and Creemers, J.W. (2004). Limited redundancy of the proprotein convertase furin in mouse liver. J. Biol. Chem. *279*, 53442–53450.

Rousselet, E., Benjannet, S., Hamelin, J., Canuel, M., and Seidah, N.G. (2011). The proprotein convertase PC7: unique zymogen activation and trafficking pathways. J. Biol. Chem. *286*, 2728–2738.

Salonikidis, P.S., Niebert, M., Ullrich, T., Bao, G., Zeug, A., and Richter, D.W. (2011). An ion-insensitive cAMP biosensor for long term quantitative ratiometric fluorescence resonance energy transfer (FRET) measurements under variable physiological conditions. J. Biol. Chem. *286*, 23419–23431.

Sanchez-Duffhues, G., Fotsis, T., and ten Dijke, P. (2015). Signal Transduction: Gain of Activin Turns Muscle into Bone. Curr. Biol. *25*, R1136–R1138.

Scamuffa, N., Siegfried, G., Bontemps, Y., Ma, L., Basak, A., Cherel, G., Calvo, F., Seidah, N.G., and Khatib, A.-M. (2008). Selective inhibition of proprotein convertases represses the metastatic potential of human colorectal tumor cells. J. Clin. Invest. *118*, 352–363.

Schäfer, W., Stroh, A., Berghöfer, S., Seiler, J., Vey, M., Kruse, M.L., Kern, H.F., Klenk, H.D., and Garten, W. (1995). Two independent targeting signals in the cytoplasmic domain determine trans-Golgi network localization and endosomal trafficking of the proprotein convertase furin. EMBO J. *14*, 2424–2435.

Schlierf, B., Fey, G.H., Hauber, J., Hocke, G.M., and Rosorius, O. (2000). Rab11b is essential for recycling of transferrin to the plasma membrane. Exp. Cell Res. *259*, 257–265.

Seidah, N.G., and Prat, A. (2012). The biology and therapeutic targeting of the proprotein convertases. Nat. Rev. Drug Discov. *11*, 367–383.

Seidah, N.G., Mayer, G., Zaid, A., Rousselet, E., Nassoury, N., Poirier, S., Essalmani, R., and Prat, A. (2008). The activation and physiological functions of the proprotein convertases. Int. J. Biochem. Cell Biol. *40*, 1111–1125.

Srour, N., Lebel, A., McMahon, S., Fournier, I., Fugère, M., Day, R., and Dubois, C.M. (2003). TACE/ADAM-17 maturation and activation of sheddase activity require proprotein convertase activity. FEBS Lett. *554*, 275–283.

Stöckli, J., and Rohrer, J. (2004). The palmitoyltransferase of the cation-dependent mannose 6-phosphate receptor cycles between the plasma membrane and endosomes. Mol. Biol. Cell *15*, 2617–2626.

Sun, X., Essalmani, R., Seidah, N.G., and Prat, A. (2009). The proprotein convertase PC5/6 is protective against intestinal tumorigenesis: in vivo mouse model. Mol. Cancer *8*, 73.

Teuchert, M., Schäfer, W., Berghöfer, S., Hoflack, B., Klenk, H.D., and Garten, W. (1999). Sorting of furin at the trans-Golgi network. Interaction of the cytoplasmic tail sorting signals with AP-1 Golgi-specific assembly proteins. J. Biol. Chem. *274*, 8199–8207.

Theos, A.C., Truschel, S.T., Raposo, G., and Marks, M.S. (2005). The Silver locus product Pmel17/gp100/Silv/ME20: controversial in name and in function. Pigment Cell Res. *18*, 322–336.

Thomas, G. (2002). Furin at the cutting edge: from protein traffic to embryogenesis and disease. Nat. Rev. Mol. Cell Biol. *3*, 753–766.

Turpeinen, H., Kukkurainen, S., Pulkkinen, K., Kauppila, T., Ojala, K., Hytönen, V.P., and Pesu, M. (2011). Identification of proprotein convertase substrates using genome-wide expression correlation analysis. BMC Genomics *12*, 618.

van Dam, E.M., Ten Broeke, T., Jansen, K., Spijkers, P., and Stoorvogel, W. (2002). Endocytosed transferrin receptors recycle via distinct dynamin and phosphatidylinositol 3-kinase-dependent pathways. J. Biol. Chem. *277*, 48876–48883.

van de Loo, J.W.H.P., Creemers, J.W.M., Bright, N.A., Young, B.D., Roebroek, A.J.M., and Van de Ven, W.J.M. (1997). Biosynthesis, distinct post-translational modifications, and functional characterization of lymphoma proprotein convertase. J. Biol. Chem. *272*, 27116–27123.

VanEngelenburg, S.B., and Palmer, A.E. (2008). Fluorescent biosensors of protein function. Curr. Opin. Chem. Biol. *12*, 60–65.

Wan, L., Molloy, S.S., Thomas, L., Liu, G., Xiang, Y., Rybak, S.L., and Thomas, G. (1998). PACS-1 defines a novel gene family of cytosolic sorting proteins required for trans-Golgi network localization. Cell *94*, 205–216.

Wouters, S., Leruth, M., Decroly, E., Vandenbranden, M., Creemers, J.W., van de Loo, J.W., Ruysschaert, J.M., and Courtoy, P.J. (1998). Furin and proprotein convertase 7 (PC7)/lymphoma PC endogenously expressed in rat liver can be resolved into distinct post-Golgi compartments. Biochem. J. *336*, 311–316.

Xia, Z., and Liu, Y. (2001). Reliable and global measurement of fluorescence resonance energy transfer using fluorescence microscopes. Biophys. J. *81*, 2395–2402.